Letter

Identification of odd-frequency superconducting pairing in Josephson junctions

Subhajit Pal [1,*] Aabir Mukhopadhyay [1,†] Vivekananda Adak,[2,‡] and Sourin Das[1,§]
[1]*Indian Institute of Science Education and Research Kolkata, Mohanpur, Nadia 741 246, West Bengal, India*
[2]*Department of Physics, Korea Advanced Institute of Science and Technology, Daejeon 34141, Korea*

(Received 2 December 2023; revised 29 May 2024; accepted 31 May 2024; published 14 June 2024)

Optimal choice of spin polarization enables electron injection into the helical edge state at a precise position, despite the uncertainty principle, permitting access to specific nonlocal Green's functions. We show, within 1D effective description, that this fact facilitates a direct identification of odd-frequency pairing through parity measurement (under frequency reversal) of the nonlocal differential conductance in a setup comprising the Josephson junction on the helical edge state of a 2D topological insulator with two spin-polarized probes tunnel-coupled to the junction region. A 2D numerical simulation has also been conducted to confirm theoretical predictions as well as to demonstrate the experimental feasibility of the proposal.

DOI: 10.1103/PhysRevB.109.L220504

Introduction. In a conventional superconductor, electrons form Cooper pairs due to a weak attraction mediated via lattice vibrations [1]. The pairing function between the two electrons within a Cooper pair can be classified into different symmetry classes by means of four permutation operators with respect to spin (S), relative coordinate (P^*), orbital index (O), and time coordinate (T^*), all of which can only have eigenvalues ± 1. Generally, BCS theory of a single-orbital superconductor ($\langle O\rangle = 1$) is instantaneous in time ($\langle T^*\rangle = 1$). This leaves two choices for the combinations of eigenvalues of the operators S and P^* to satisfy the Berezinskii condition [2] $SP^*OT^* = -1$ for the pairing function, i.e., $\{\langle S\rangle, \langle P^*\rangle\} = \{-1, 1\}, \{1, -1\}$. These correspond to spin-singlet even-parity (e.g., s-wave) and spin-triplet odd-parity [3] (e.g., p-wave) symmetries, respectively. If one removes the constraint of instantaneous pairing, the possibility of temporal (nonlocal in time) Cooper pairing becomes feasible, and both $\langle T^*\rangle = \pm 1$ can be possible, depending on whether the pairing function is symmetric or antisymmetric under the permutation of relative time coordinates of the electrons forming the Cooper pair. Temporally symmetric pairing ($\langle T^*\rangle = 1$) does not give rise to any new symmetry classes other than those already described by BCS theory and is generally known as even-frequency (even-ω) pairing. However, temporally antisymmetric pairing ($\langle T^*\rangle = -1$), which is known as odd-frequency (odd-ω) pairing [4–6], opens up possibilities of two new symmetry classes (assuming $\langle O\rangle = 1$) that cannot be described by BCS theory, namely, spin-singlet odd-parity ($\{\langle S\rangle, \langle P^*\rangle\} = \{-1, -1\}$) and spin-triplet even-parity ($\{\langle S\rangle, \langle P^*\rangle\} = \{1, 1\}$) pairings, consistent with the Berezinskii condition. It can also be shown that this odd-ω (even-ω) pairing is also odd (even) under the sign change of energy [4], which gives the advantage of observing the behavior of this pairing in the energy domain rather than in the temporal domain.

On a historical note, the concept of odd-ω spin-triplet pairing traces back to Berezinskii's 1974 proposal in ^{3}He [2] and predictions in disordered systems [7,8]. Balatsky and Abrahams later indicated the presence of odd-ω spin-singlet pairing in time-reversal and parity symmetry broken superconductors [9]. Subsequently, the odd-ω pairing was explored within the framework of a two-channel Kondo system [10], the 1D t-J-h model [11], the 2D Hubbard model [12], and heavy-fermion compounds [13]. The bulk odd-ω pairing has been indirectly hinted theoretically through the Majorana scanning tunneling microscope [14] and also experimentally using the Kerr effect [15,16] and the paramagnetic Meissner effect [17–21]. Further, the evidence of bulk odd-ω pairing due to magnetic impurities has emerged in s-wave superconductors [22,23]. In Ref. [24], a measurement tool was introduced for directly detecting odd-ω pairing in bulk systems using time- and angle-resolved photoelectron fluctuation spectroscopy. However, this method requires advanced technology beyond the current capabilities of facilities. More recently, in Ref. [25], the authors proposed a detection scheme to directly identify odd-ω pairing in bulk systems using the quasiparticle interference method in the presence of an external magnetic field. Initially, odd-ω pairing was regarded as an inherent bulk phenomenon [2,9,26] but was subsequently acknowledged to manifest in heterojunctions [27–55] and in the systems under the influence of time-dependent fields [56,57]. Certain theoretical studies have indirectly identified odd-ω pairing in heterostructures. For instance, this was achieved through phase-tunable electron transport in topological Josephson junctions (JJs) [58], examining Josephson current characteristics on the surface of Weyl nodal loop semimetals [59], and analyzing current noise in JJs [60]. Experimental evidence of odd-ω pairing in heterostructures emerged through measurements of long-range supercurrents in magnetic JJs [61,62]. These two experiments utilize a ferromagnetic material to create an odd-ω pairing effect, which is subsequently identified by measuring long-range

*Contact author: subhajitp778@gmail.com
†Contact author: aabir.riku@gmail.com
‡Contact author: adakvivek0705@gmail.com
§Contact author: sourin@iiserkol.ac.in

superconducting pairing. In contrast, this Letter investigates a configuration that inherently supports odd-ω pairing without the need for any ferromagnet/superconductor junction. A topological JJ at the edge of a two-dimensional (2D) quantum spin Hall insulator (QSHI) serves this purpose. It is important to mention here that induced superconductivity in the QSHI edge has already been experimentally demonstrated [63].

We demonstrate that it is possible to read off all the independent, spatially nonlocal Green's functions by measuring differential conductance between two spin-polarized probes placed at the junction. The underlying interplay between spin-momentum locking of helical edge states (HESs) and spin-polarization of the probes allows for this advantage. Experimentally, the injection of spin-polarized current into the HESs of QSHIs has already been achieved [64]. By using spin-polarized probes, one can inject (detect) electrons into (from) the helical edge with well-defined position and momentum simultaneously, which, in general, is prohibited due to the uncertainty principle [65]. To elaborate further, a spin-$\uparrow$ (spin-$\downarrow$) electron injected at position x in the helical edge can only tunnel into the right (left) moving edge mode owing to spin-momentum locking. Keeping the spin-polarization axes of the tunneling probes aligned parallel or antiparallel to the spin-quantization axis of HESs, we study the difference between nonlocal differential conductance from the left probe to right probe $\kappa^{21}_{s\bar{s}}(V,0)$ and from the right probe to left probe $\kappa^{12}_{\bar{s}s}(0,V)$, i.e.,

$$\begin{aligned}\mathcal{A}^{2,1}_{s,\bar{s}} &= \kappa^{21}_{s\bar{s}}(V_1 = V, V_2 = 0) - \kappa^{12}_{\bar{s}s}(V_1 = 0, V_2 = V) \\ &= \left[\frac{dI^{21}_{s\bar{s}}}{dV}\right]_{(V_1=V,V_2=0)} - \left[\frac{dI^{12}_{\bar{s}s}}{dV}\right]_{(V_1=0,V_2=V)}, \end{aligned} \tag{1}$$

where $\{s,\bar{s}\} \in \{\uparrow,\downarrow\}$ with $s \neq \bar{s}$, and V_1 (V_2) denotes the applied voltage at the left (right) tunneling probe P_1 (P_2). It can be shown that this quantity $\mathcal{A}^{2,1}_{s,\bar{s}}$ can be written as a product of odd-ω and even-ω pairing amplitudes and hence should be odd with respect to incident energy (and hence with respect to the applied voltage V). We show that this difference stems from the same origin as that of the odd-ω part of the nonlocal differential conductance, which can be accessed via bias reversal, i.e., $\mathcal{B}^{2,1}_{s,\bar{s}} = \kappa^{21}_{s\bar{s}}(V,0) - \kappa^{21}_{s\bar{s}}(-V,0)$. This fact leads to

$$\mathcal{A}^{2,1}_{s,\bar{s}} = \mathcal{B}^{2,1}_{s,\bar{s}}. \tag{2}$$

From an experimental perspective, measuring the antisymmetric behavior of each of these independent quantities and their equality confirms the existence of odd-ω pairing. In what follows, we will first present our results using an effective 1D analytic model of the HES. Following that, we will provide a 2D simulation of a realistic setup, in line with HgTe/CdTe quantum well parameters, confirming our predictions.

Model and its motivation. The system we are interested in is a JJ of length L ($0 \leqslant x \leqslant L$), realized in a HES of a 2D QSHI [66–70] (1D Dirac fermions) which is proximitized to a conventional s-wave superconductor. A schematic of the setup is shown in Fig. 1(a), while Fig. 1(b) shows the corresponding simplified cartoon representation of the same setup. The Bogoliubov–de Gennes (BdG) Hamiltonian characterizing such junctions can be written as [71,72] $H_J = \int_{-\infty}^{\infty} dx\, \Psi^\dagger \mathcal{H}_J \Psi$ where $\Psi = (\psi_\uparrow, \psi_\downarrow, \psi^\dagger_\downarrow, -\psi^\dagger_\uparrow)^T$ is the

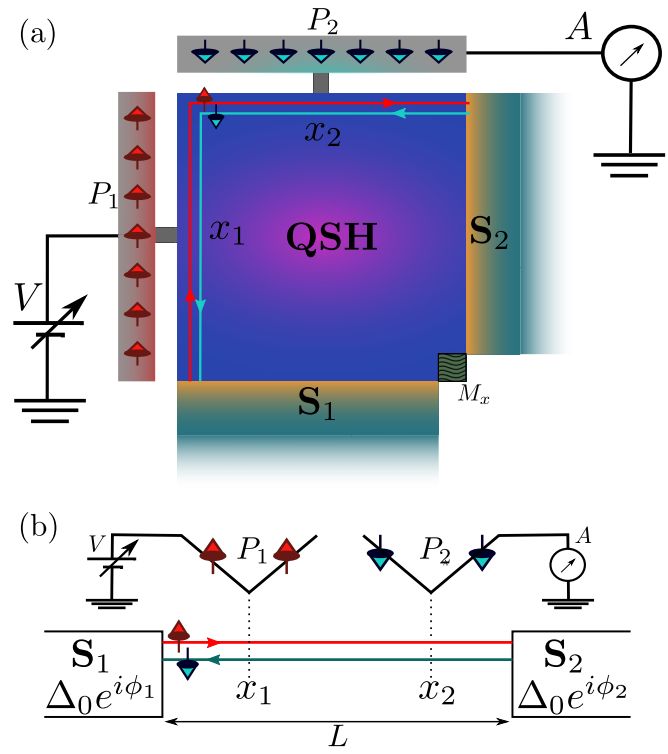

FIG. 1. (a) Schematic of the setup consisting of a Josephson junction at the edge of a 2D QSHI with two spin-polarized tunneling probes (P_1 and P_2) at $x = x_1$ and $x = x_2$. Up and down arrows represent the spin polarization direction of helical edge states as well as of the spin-polarized tunneling probes. A bias voltage V is applied to P_1 while the current through P_2 is measured by the current readout device A. (b) A simplified cartoon representation of the above setup.

Nambu basis and

$$\mathcal{H}_J = -i\hbar v_F \partial_x \tau_z \sigma_z - \mu\tau_z + \Delta(x)(\cos\varphi_r \tau_x - \sin\varphi_r \tau_y). \tag{3}$$

Here, σ_i and τ_i are the Pauli matrices acting respectively on the spin basis and particle-hole basis, μ is the chemical potential of the HES, v_F represents the Fermi velocity of the HES, and $\hat{p} = -i\hbar\partial_x$ is the momentum operator. The spin-quantization axis of the HES is considered to be along the z direction [71,72]. The superconducting pairing potential is given by $\Delta(x) = \Delta_0[\Theta(-x) + \Theta(x - L)]$. Superconducting leads (S_r) are identified as $r \in \{1,2\}$ with the corresponding superconducting phases φ_r such that the superconducting phase difference $\varphi_{21} = \varphi_2 - \varphi_1 \neq 0$, in general.

Two spin-polarized tunneling probes [73] $P_{\{1,2\}}$ (P_r being closer to S_r) with spin-polarization axes oriented respectively along $\hat{n}_1$ and $\hat{n}_2$, at angles θ_1 and θ_2 with respect to the spin-quantization axis of the HES (say, in the z-x plane) [74], are introduced at positions $x = x_1$ and $x = x_2$, respectively, within the junction region ($0 < x_1 < x_2 < L$). For most of this Letter, we will only be discussing the case for $\{\theta_1,\theta_2\} = \{0,\pi\}$, unless otherwise stated. To keep the algebra simple while retaining the essential physical inputs, we model the probes as a spin-polarized 1D mode. The second quantized Hamiltonians of these probes can be expressed as

$$H_{P_{1(2)}} = -i\hbar v_F \int_{-\infty}^{\infty} d\tilde{x} \left(\psi^\dagger_{\hat{n}_{1(2)}} \partial_{\tilde{x}} \psi_{\hat{n}_{1(2)}}\right). \tag{4}$$

TABLE I. Output at P_2 (P_1) when an electron is injected into the HES through P_1 (P_2) and the corresponding Green's functions depending on the polarization of the tunneling probes.

Input at P_1	Polarization of $P_1(\theta_1)$	Polarization of $P_2(\theta_2)$	Output at P_2	Contributing Green's function	Input at P_2	Polarization of $P_2(\theta_2)$	Polarization of $P_1(\theta_1)$	Output at P_1	Contributing Green's function
e	↑	↑	e	$G^{r(a)}_{ee,\uparrow\uparrow}(x_2 > x_1)$	e	↑	↑	e	$G^{r(a)}_{ee,\uparrow\uparrow}(x_1 < x_2)$
e	↑	↓	h	$G^{r(a)}_{he,\downarrow\uparrow}(x_2, x_1)$	e	↑	↓	h	$G^{r(a)}_{he,\downarrow\uparrow}(x_1, x_2)$
e	↓	↑	h	$G^{r(a)}_{he,\uparrow\downarrow}(x_2, x_1)$	e	↓	↑	h	$G^{r(a)}_{he,\uparrow\downarrow}(x_1, x_2)$
e	↓	↓	e	$G^{r(a)}_{ee,\downarrow\downarrow}(x_2 > x_1)$	e	↓	↓	e	$G^{r(a)}_{ee,\downarrow\downarrow}(x_1 < x_2)$

The tunneling Hamiltonian between the HES and the probes can be written as

$$H_T^{P_i} = \hbar v_F \int_{-\infty}^{\infty} dx\, \delta(x - x_i) \left(\sum_{\substack{\alpha,\alpha' \\ \alpha \neq \alpha'}} t^i_{\alpha\alpha'} \psi^\dagger_\alpha \psi_{\alpha'} + \text{H.c.} \right) \quad (5)$$

with $\alpha, \alpha' \in \{\uparrow, \downarrow, \hat{n}_i\}$ ($\alpha \neq \alpha'$ and $i \in \{1, 2\}$). $t^i_{\alpha\alpha'} = t_i \gamma_{\alpha\alpha'}$ is the tunneling strength between α and α' at $x = x_i$ and $\gamma_{\alpha\alpha'}$ is the overlap of the spinor part of the first quantized wave function of electrons in the probes and the HES. From this point onward, we shall consider $\hbar = v_F = 1$. Note that this form of tunneling respects $SU(2)$ symmetry and hence cannot induce spin-flip scattering when n_i is parallel or antiparallel to the spin-quantization axis of the HES. Using the equation of motion approach for the Hamiltonian $H = H_{\text{HES}} + \sum_{i\in\{1,2\}} H_{P_i} + H_T^{P_i}$ (where $H_{\text{HES}} = H_J|_{\Delta=0}$), the scattering matrices can be expressed as

$$\psi^{\text{out}}_\alpha(x_i) = \sum_{\alpha'} S^e_{\alpha\alpha'}(x_i) \psi^{\text{in}}_{\alpha'}(x_i), \quad (6)$$

where $\psi^{\text{in(out)}}$ are the corresponding incoming (outgoing) plane wave amplitudes on the HES and the probe. The scattering matrix for holes (S^h) can be determined by exploiting the particle-hole symmetry of the system (for details, see Supplemental Material (SM) [75], Sec. A). We are interested in studying charge transport between the two probes via the junction when a finite voltage bias V is applied such that $-\Delta_0 \leqslant eV \leqslant \Delta_0$.

Note that the spatial nonlocality of the probes, along with the helical nature of the edge state, opens up the possibility of detecting only a hole at P_2 when an electron is injected into HES through P_1 provided the polarization of the probes is tuned such that $\theta_1, \theta_2 = 0$ or π and $\theta_1 \neq \theta_2$. This leads to the fact that the differential conductance between the probes is directly proportional to the square of the modulus of anomalous Green's functions. This can be understood in terms of a simple process, as described below. If the spin polarization of P_1 is set to spin-↑ (i.e., $\theta_1 = 0$), it can only inject a right-moving electron to the HES due to the spin-momentum locking of the edge states. In the absence of spin-flip scattering within the HES, this electron will either remain as a spin-↑ electron after an even number of Andreev reflections (including the possibility of no Andreev reflection) or will convert to a spin-↓ hole after an odd number of Andreev reflections when it reaches $x = x_2$. Thus, P_2 will detect only a hole for $\theta_2 = \pi$. Along the same line of argument, it is straightforward to show that for $\theta_2 = 0$, P_2 will detect only an electron. By definition, the probability amplitude of these nonlocal transmissions will be proportional to the corresponding Green's functions, namely $t^{21}_{ee,\uparrow\uparrow} \propto G^{r(a)}_{ee,\uparrow\uparrow}(x_2 > x_1)$ and $t^{21}_{he,\downarrow\uparrow} \propto G^{r(a)}_{he,\downarrow\uparrow}(x_2, x_1)$, where $t^{21}_{ee,\uparrow\uparrow}$ and $t^{21}_{he,\downarrow\uparrow}$ are the propagation amplitudes for spin-up electron and spin-down hole, respectively, from the left probe to the right probe, and $G^{r(a)}_{ee,s_2s_1}(x_2 > x_1)$ represents the retarded (advanced) normal Green's functions while $G^{r(a)}_{he,s_2s_1}(x_2, x_1)$ ($s_i \in \{\uparrow, \downarrow\}$) denotes the retarded (advanced) anomalous Green's functions calculated at $x = x_2$. Here retarded and advanced Green's functions are defined in the appropriate frequency domain [38]. The above discussion is summarized in the form of Table I.

Using Landauer's formula [76], we can calculate the differential conductance from P_1 to P_2, given by $\kappa^{21}_{\downarrow\uparrow} = \kappa^{21}_{ee,\downarrow\uparrow} - \kappa^{21}_{he,\downarrow\uparrow}$, and from P_2 to P_1, given by $\kappa^{12}_{\uparrow\downarrow} = \kappa^{12}_{ee,\uparrow\downarrow} - \kappa^{12}_{he,\uparrow\downarrow}$, where $\kappa^{ij}_{p_ip_j,s_is_j} = (e^2/h)|t^{ij}_{p_ip_j,s_is_j}|^2$ ($p_{i(j)} \in \{e, h\}$, $s_{i(j)} \in \{\uparrow, \downarrow\}$, $\{i, j\} \in \{1, 2\}$). The difference between these two nonlocal differential conductances at energy (frequency) ω is given by

$$\begin{aligned} \mathcal{A}^{2,1}_{\downarrow,\uparrow} &= \kappa^{21}_{\downarrow\uparrow} - \kappa^{12}_{\uparrow\downarrow} = -\kappa^{21}_{he,\downarrow\uparrow} + \kappa^{12}_{he,\uparrow\downarrow}, \\ &\propto -\left|G^r_{he,\downarrow\uparrow}(x_2, x_1, \omega)\right|^2 + \left|G^r_{he,\uparrow\downarrow}(x_1, x_2, \omega)\right|^2, \\ &\propto -\left|G^r_{he,\downarrow\uparrow}(x_2, x_1, \omega)\right|^2 + \left|G^a_{he,\downarrow\uparrow}(x_2, x_1, -\omega)\right|^2, \\ &\propto \text{Re}\left[\mathcal{O}\left[G^r_{he,\downarrow\uparrow}(x_2, x_1, \omega)\right] \times \mathcal{E}\left[G^{r*}_{he,\downarrow\uparrow}(x_2, x_1, \omega)\right]\right], \end{aligned} \quad (7)$$

where we have used the property $G^r_{he,s\bar{s}}(x, x', \omega) = G^a_{he,\bar{s}s}(x', x, -\omega)$ ($\{s, \bar{s}\} \in \{\uparrow, \downarrow\}$ and $s \neq \bar{s}$). Here we have used only retarded Green's functions to express κ. However, a proof involving advanced Green's functions follows in a similar way (see SM [75], Sec. B). In Eq. (7), $\mathcal{A}^{2,1}_{\downarrow,\uparrow}$ is *antisymmetric* with respect to ω, and if measured, it can be treated as a direct signature of odd-ω pairing subjected to the condition that even-ω pairing within the junction is nonzero. In Eq. (7), $\mathcal{O}$ and $\mathcal{E}$ denote the odd-in-ω (antisymmetric with respect to ω) and even-in-ω (symmetric with respect to ω) parts of the corresponding Green's functions which are in turn directly related to odd-ω and even-ω pairing amplitudes, respectively. Note that the quantity in Eq. (7) can also be expressed as $\mathcal{B}^{2,1}_{\downarrow,\uparrow} = [\kappa^{21}_{\downarrow\uparrow}(\omega) - \kappa^{21}_{\downarrow\uparrow}(-\omega)]$. The voltage configuration necessary for measuring $\mathcal{A}$ and $\mathcal{B}$ is discussed above Eq. (2). It is worth mentioning that the Green's functions discussed above are not, in general, the free

Green's function of the JJ, i.e., the Green's functions in the absence of tunneling probes. However, in the weak-tunneling limit ($t_1, t_2 \ll 1$), different interlead transmission amplitudes can be written in terms of free Green's functions (for details see SM [75], Sec. C). Next, we will proceed to put the above qualitative discussion on firm grounds by calculating the quantity $\mathcal{A}^{2,1}_{\downarrow,\uparrow}$ from numerical analysis using a 2D model, and comparing the theoretical results discussed above (and also results presented in the SM [75]).

Numerical simulation using 2D model. In this part, we conduct a numerical simulation of a 2D lattice model depicted in Fig. 1 using the KWANT package [77] to further analyze the effective 1D model discussed above. The system is mainly a QSHI which is described by a real-space configuration of the Bernevig-Hughes-Zhang (BHZ) model [78] mapped on a square lattice of dimension $140a \times 140a$ with additional terms incorporated as needed. Here a (=3 nm) is the lattice spacing. Two superconducting leads are attached to the bottom side (S_1) and to the right side (S_2) of the system, which are defined by the s-wave superconductivity-proximitized QSHIs [79] having a finite phase difference ($\phi_{21} = \phi_2 - \phi_1$) between them and thus defining a 1D JJ extended over the left and top edges of the QSH region [see Fig. 1(a)]. On the other hand, two spin-polarized normal leads, which can be described by two quantum anomalous Hall insulators carrying chiral edge states of opposite chiralities, are tunnel-coupled via tiny insulating sections to the left side (P_1: having the $\uparrow$-spin channel only) and to the top side (P_2: having only the $\downarrow$-spin channel) of the QSH region. The quantum anomalous Hall state of a spin-polarized lead is obtained by applying an exchange field to the QSH system, which oppositely affects the effective bulk gaps for the two spin states, eventually, at sufficient strength, destroying the topological state for one of them [80]. A strong on-site ferromagnetic impurity term is added over a small section of dimension $14a \times 14a$ at the extreme bottom-right corner (denoted by M_x) of the QSH region to ensure that the current is allowed to propagate only through the left and top edges of the QSH region in between S_1 and S_2. A detailed insight into the 2D simulation is closely comparable to the same discussed in Ref. [81] along with a comprehensive understanding of how particle-hole symmetry can be incorporated into the lattice model [82]. For the numerical calculation, we consider the value of chemical potential (μ) to be zero and the s-wave superconducting pairing potential (Δ_0) as 2.0 meV. The values of the remaining parameters related to the BHZ model closely resemble those describing HgTe/CdTe quantum wells [78,81,82]. Finally, by conducting a numerical simulation with this setup, we compute the quantity $\mathcal{A}^{2,1}_{\downarrow,\uparrow}$ for $\phi_{21} = \pi/2$ as shown in Fig. 2 (solid cream-colored line). The insulating necks of P_1 and P_2 are considered to be identical.

To compare the numerical result with the theoretical result, one needs to estimate the values of L, t_1, and t_2. To estimate the value of L, we analyzed the positions of the peaks and dips of $\mathcal{A}^{2,1}_{\downarrow,\uparrow}$. By mapping the corresponding energy values to the Andreev bound state (ABS) energies, we estimate $L = 4.35\xi$ where $\xi = \hbar v_F/\Delta_0$ is the superconducting coherence length. Plugging this value of L into theoretical calculations

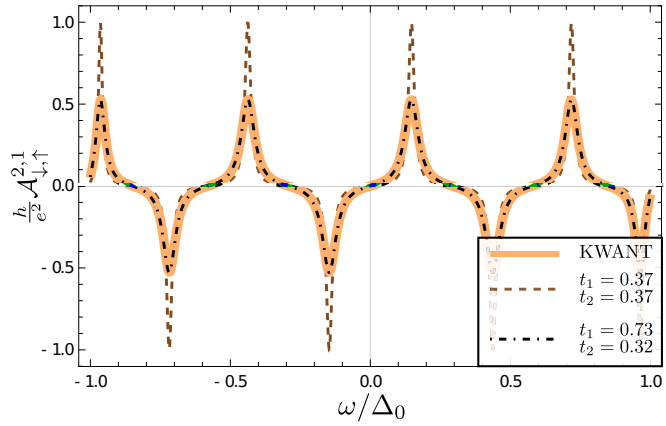

FIG. 2. Antisymmetry in nonlocal differential conductance $\mathcal{A}^{2,1}_{\downarrow,\uparrow}$ as a function of $\omega = eV$, where V is the applied bias voltage. Parameters are $\mu = 0$, $\phi_{21} = \pi/2$, $L = 4.35\xi$, $\theta_1 = 0$, $\theta_2 = \pi$.

we numerically calculated the following quantity:

$$\delta = \frac{1}{N}\sqrt{\sum_{n=1}^{N}[\mathcal{A}^{2,1}_{\downarrow,\uparrow}(n)|_{\text{Analytical}} - \mathcal{A}^{2,1}_{\downarrow,\uparrow}(n)|_{\text{Numerical}}]^2}, \quad (8)$$

for different values of t_1 and t_2. Here N is the number of numerical grids within the energy window $-\Delta_0 \leqslant \omega \leqslant \Delta_0$. Keeping the tunneling strengths the same, it turns out that $\delta_{\min} \approx 2 \times 10^{-3}$ for $t_1 = t_2 = 0.37$ (dashed brown line in Fig. 2). Although this plot is a good fit to the numerical results, if we relax the condition of $t_1 = t_2$, then the value of δ can be even minimized giving rise to a better fit to the numerical results. It turns out that $\delta_{\min} \approx 1 \times 10^{-4}$ for $t_1 = 0.73$ and $t_2 = 0.32$ (black dot-dashed line in Fig. 2). The dependence of $\mathcal{A}$ on the system parameters t_1, t_2, and L is shown in the SM [75], Sec. D.

Discussion. The above results rely on the fact that the spin-polarization axes of P_1 and P_2 can be adjusted exactly parallel or antiparallel to the spin-polarization axis of the HES. For any other values of θ_1 and θ_2, $\mathcal{A}$ will have contributions from interference effects between the spin channels and the electron-hole channels due to the presence of more than one Green's function in the expressions of $t^{ij}_{p\bar{p}}$. These interference contributions will lead to the deviation from perfectly antisymmetric features. Also, the detection of odd-frequency pairing through $\mathcal{A}$ does not require the probes P_1 and P_2 to be placed at different positions. This is due to the fact that the information of position enters into the calculation as pure phase contributions to $t^{ij}_{p\bar{p},s\bar{s}}$ ($\{s, \bar{s}\} \in \{\uparrow, \downarrow\}$, $s \neq \bar{s}$).

In our proposed setup, the size of the sample (i.e., the length of the junction L) should be large enough to accommodate two spin-polarized probes. In Ref. [64], the width of the spin-polarized probe tip is 0.77 μm, which sets the minimum dimension of the quantum spin Hall sample (length of the edge) to be 1.54 μm. However, in the same experiment, the size of the sample (length of the edge) is 4.1 μm. Thus, it should be possible to experimentally fabricate a similar

sample to realize our proposal. The values of other model parameters, e.g., the Fermi velocity v_F, the chemical potential μ, and the pairing term Δ can be estimated from the experiment [63].

Lastly, note that $\kappa^{21}_{he,\downarrow\uparrow}$ is related to the ABS corresponding to the shuttling of a Cooper pair from left to right, while $\kappa^{12}_{he,\uparrow\downarrow}$ is related to the ABS corresponding to the shuttling of the Cooper pair in the opposite direction. Thus, in the weak-tunneling limit, at $\varphi_{21} = 0$ or π (when these two ABSs become degenerate), the differential conductances $\kappa^{21}_{he,\downarrow\uparrow}$ and $\kappa^{12}_{he,\uparrow\downarrow}$ become equal, leading to the vanishing of $\mathcal{A}^{2,1}_{\downarrow,\uparrow}$.

Acknowledgments. S.P. and A.M. acknowledge the Ministry of Education, India, and IISER Kolkata for funding. V.A. would like to acknowledge Korea NRF (SRC Center for Quantum Coherence in Condensed Matter, Grant No. RS-2023-00207732) for funding.

S.P. and A.M. contributed equally to this work.

[1] J. Bardeen, L. N. Cooper, and J. R. Schrieffer, Theory of superconductivity, Phys. Rev. **108**, 1175 (1957).

[2] V. Berezinskii, New model of the anisotropic phase of superfluid He^3, JETP Lett. **20**, 287 (1974).

[3] M. Sigrist and K. Ueda, Phenomenological theory of unconventional superconductivity, Rev. Mod. Phys. **63**, 239 (1991).

[4] J. Linder and A. V. Balatsky, Odd-frequency superconductivity, Rev. Mod. Phys. **91**, 045005 (2019).

[5] Y. Tanaka, M. Sato, and N. Nagaosa, Symmetry and topology in superconductors: Odd-frequency pairing and edge states, J. Phys. Soc. Jpn. **81**, 011013 (2012).

[6] J. Cayao, C. Triola, and A. M. Black-Schaffer, Odd-frequency superconducting pairing in one-dimensional systems, Eur. Phys. J.: Spec. Top. **229**, 545 (2020).

[7] T. R. Kirkpatrick and D. Belitz, Disorder-induced triplet superconductivity, Phys. Rev. Lett. **66**, 1533 (1991).

[8] D. Belitz and T. R. Kirkpatrick, Even-parity spin-triplet superconductivity in disordered electronic systems, Phys. Rev. B **46**, 8393 (1992).

[9] A. Balatsky and E. Abrahams, New class of singlet superconductors which break the time reversal and parity, Phys. Rev. B **45**, 13125 (1992).

[10] V. J. Emery and S. Kivelson, Mapping of the two-channel Kondo problem to a resonant-level model, Phys. Rev. B **46**, 10812 (1992).

[11] A. V. Balatsky and J. Bonča, Even- and odd-frequency pairing correlations in the one-dimensional *t-J-h* model: A comparative study, Phys. Rev. B **48**, 7445 (1993).

[12] N. Bulut, D. J. Scalapino, and S. R. White, Effective particle-particle interaction in the two-dimensional Hubbard model, Phys. Rev. B **47**, 6157 (1993).

[13] P. Coleman, E. Miranda, and A. Tsvelik, Possible realization of odd-frequency pairing in heavy fermion compounds, Phys. Rev. Lett. **70**, 2960 (1993).

[14] O. Kashuba, B. Sothmann, P. Burset, and B. Trauzettel, Majorana STM as a perfect detector of odd-frequency superconductivity, Phys. Rev. B **95**, 174516 (2017).

[15] E. Schemm, W. Gannon, C. Wishne, W. Halperin, and A. Kapitulnik, Observation of broken time-reversal symmetry in the heavy-fermion superconductor UPt_3, Science **345**, 190 (2014).

[16] L. Komendová and A. M. Black-Schaffer, Odd-frequency superconductivity in Sr_2RuO_4 measured by Kerr rotation, Phys. Rev. Lett. **119**, 087001 (2017).

[17] A. Di Bernardo, Z. Salman, X. L. Wang, M. Amado, M. Egilmez, M. G. Flokstra, A. Suter, S. L. Lee, J. H. Zhao, T. Prokscha, E. Morenzoni, M. G. Blamire, J. Linder, and J. W. A. Robinson, Intrinsic paramagnetic Meissner effect due to *s*-wave odd-frequency superconductivity, Phys. Rev. X **5**, 041021 (2015).

[18] F. S. Bergeret, A. F. Volkov, and K. B. Efetov, Josephson current in superconductor-ferromagnet structures with a nonhomogeneous magnetization, Phys. Rev. B **64**, 134506 (2001).

[19] M. Alidoust, K. Halterman, and J. Linder, Meissner effect probing of odd-frequency triplet pairing in superconducting spin valves, Phys. Rev. B **89**, 054508 (2014).

[20] J. A. Krieger, A. Pertsova, S. R. Giblin, M. Döbeli, T. Prokscha, C. W. Schneider, A. Suter, T. Hesjedal, A. V. Balatsky, and Z. Salman, Proximity-induced odd-frequency superconductivity in a topological insulator, Phys. Rev. Lett. **125**, 026802 (2020).

[21] T. Yokoyama, Y. Tanaka, and N. Nagaosa, Anomalous Meissner effect in a normal-metal–superconductor junction with a spin-active interface, Phys. Rev. Lett. **106**, 246601 (2011).

[22] V. Perrin, F. L. N. Santos, G. C. Ménard, C. Brun, T. Cren, M. Civelli, and P. Simon, Unveiling odd-frequency pairing around a magnetic impurity in a superconductor, Phys. Rev. Lett. **125**, 117003 (2020).

[23] D. Kuzmanovski, R. S. Souto, and A. V. Balatsky, Odd-frequency superconductivity near a magnetic impurity in a conventional superconductor, Phys. Rev. B **101**, 094505 (2020).

[24] V. Kornich, F. Schlawin, M. A. Sentef, and B. Trauzettel, Direct detection of odd-frequency superconductivity via time- and angle-resolved photoelectron fluctuation spectroscopy, Phys. Rev. Res. **3**, L042034 (2021).

[25] D. Chakraborty and A. M. Black-Schaffer, Quasiparticle interference as a direct experimental probe of bulk odd-frequency superconducting pairing, Phys. Rev. Lett. **129**, 247001 (2022).

[26] E. Abrahams, A. Balatsky, D. J. Scalapino, and J. R. Schrieffer, Properties of odd-gap superconductors, Phys. Rev. B **52**, 1271 (1995).

[27] F. S. Bergeret, A. F. Volkov, and K. B. Efetov, Long-range proximity effects in superconductor-ferromagnet structures, Phys. Rev. Lett. **86**, 4096 (2001).

[28] F. S. Bergeret, A. F. Volkov, and K. B. Efetov, Manifestation of triplet superconductivity in superconductor-ferromagnet structures, Phys. Rev. B **68**, 064513 (2003).

[29] F. S. Bergeret, A. F. Volkov, and K. B. Efetov, Odd triplet superconductivity and related phenomena in superconductor-ferromagnet structures, Rev. Mod. Phys. **77**, 1321 (2005).

[30] M. Eschrig, J. Kopu, J. C. Cuevas, and G. Schön, Theory of half-metal/superconductor heterostructures, Phys. Rev. Lett. **90**, 137003 (2003).

[31] A. F. Volkov, A. Anishchanka, and K. B. Efetov, Odd triplet superconductivity in a superconductor/ferromagnet system with a spiral magnetic structure, Phys. Rev. B **73**, 104412 (2006).
[32] T. Yokoyama, Y. Tanaka, and A. A. Golubov, Manifestation of the odd-frequency spin-triplet pairing state in diffusive ferromagnet/superconductor junctions, Phys. Rev. B **75**, 134510 (2007).
[33] Y. Tanaka, Y. Tanuma, and A. A. Golubov, Odd-frequency pairing in normal-metal/superconductor junctions, Phys. Rev. B **76**, 054522 (2007).
[34] A. M. Black-Schaffer and A. V. Balatsky, Odd-frequency superconducting pairing in topological insulators, Phys. Rev. B **86**, 144506 (2012).
[35] A. M. Black-Schaffer and A. V. Balatsky, Proximity-induced unconventional superconductivity in topological insulators, Phys. Rev. B **87**, 220506(R) (2013).
[36] F. Crépin, P. Burset, and B. Trauzettel, Odd-frequency triplet superconductivity at the helical edge of a topological insulator, Phys. Rev. B **92**, 100507(R) (2015).
[37] P. Burset, B. Lu, G. Tkachov, Y. Tanaka, E. M. Hankiewicz, and B. Trauzettel, Superconducting proximity effect in three-dimensional topological insulators in the presence of a magnetic field, Phys. Rev. B **92**, 205424 (2015).
[38] J. Cayao and A. M. Black-Schaffer, Odd-frequency superconducting pairing and subgap density of states at the edge of a two-dimensional topological insulator without magnetism, Phys. Rev. B **96**, 155426 (2017).
[39] S.-Y. Hwang, P. Burset, and B. Sothmann, Odd-frequency superconductivity revealed by thermopower, Phys. Rev. B **98**, 161408(R) (2018).
[40] J. Cayao and A. M. Black-Schaffer, Odd-frequency superconducting pairing in junctions with Rashba spin-orbit coupling, Phys. Rev. B **98**, 075425 (2018).
[41] J. Linder, A. Sudbø, T. Yokoyama, R. Grein, and M. Eschrig, Signature of odd-frequency pairing correlations induced by a magnetic interface, Phys. Rev. B **81**, 214504 (2010).
[42] J. Linder, T. Yokoyama, A. Sudbø, and M. Eschrig, Pairing symmetry conversion by spin-active interfaces in magnetic normal-metal–superconductor junctions, Phys. Rev. Lett. **102**, 107008 (2009).
[43] S. Pal and C. Benjamin, Exciting odd-frequency equal-spin triplet correlations at metal-superconductor interfaces, Phys. Rev. B **104**, 054519 (2021).
[44] S. Tamura, Y. Tanaka, and T. Yokoyama, Generation of polarized spin-triplet Cooper pairings by magnetic barriers in superconducting junctions, Phys. Rev. B **107**, 054501 (2023).
[45] Y. Tanaka and A. A. Golubov, Theory of the proximity effect in junctions with unconventional superconductors, Phys. Rev. Lett. **98**, 037003 (2007).
[46] M. Eschrig, T. Löfwander, T. Champel, J. Cuevas, J. Kopu, and G. Schön, Symmetries of pairing correlations in superconductor-ferromagnet nanostructures, J. Low Temp. Phys. **147**, 457 (2007).
[47] A. F. Volkov, F. S. Bergeret, and K. B. Efetov, Odd triplet superconductivity in superconductor-ferromagnet multilayered structures, Phys. Rev. Lett. **90**, 117006 (2003).
[48] Y. V. Fominov, A. F. Volkov, and K. B. Efetov, Josephson effect due to the long-range odd-frequency triplet superconductivity in SFS junctions with Néel domain walls, Phys. Rev. B **75**, 104509 (2007).
[49] A. I. Buzdin, Proximity effects in superconductor-ferromagnet heterostructures, Rev. Mod. Phys. **77**, 935 (2005).
[50] A. Tsintzis, A. M. Black-Schaffer, and J. Cayao, Odd-frequency superconducting pairing in Kitaev-based junctions, Phys. Rev. B **100**, 115433 (2019).
[51] Y. Asano and Y. Tanaka, Majorana fermions and odd-frequency Cooper pairs in a normal-metal nanowire proximity-coupled to a topological superconductor, Phys. Rev. B **87**, 104513 (2013).
[52] D. Kuzmanovski and A. M. Black-Schaffer, Multiple odd-frequency superconducting states in buckled quantum spin Hall insulators with time-reversal symmetry, Phys. Rev. B **96**, 174509 (2017).
[53] C. Fleckenstein, N. T. Ziani, and B. Trauzettel, Conductance signatures of odd-frequency superconductivity in quantum spin Hall systems using a quantum point contact, Phys. Rev. B **97**, 134523 (2018).
[54] Y. Tanaka and S. Tamura, Theory of surface Andreev bound states and odd-frequency pairing in superconductor junctions, J. Supercond. Novel Magn. **34**, 1677 (2021).
[55] Y. Tanaka, A. A. Golubov, S. Kashiwaya, and M. Ueda, Anomalous Josephson effect between even- and odd-frequency superconductors, Phys. Rev. Lett. **99**, 037005 (2007).
[56] C. Triola and A. V. Balatsky, Odd-frequency superconductivity in driven systems, Phys. Rev. B **94**, 094518 (2016).
[57] C. Triola and A. V. Balatsky, Pair symmetry conversion in driven multiband superconductors, Phys. Rev. B **95**, 224518 (2017).
[58] J. Cayao, P. Dutta, P. Burset, and A. M. Black-Schaffer, Phase-tunable electron transport assisted by odd-frequency Cooper pairs in topological Josephson junctions, Phys. Rev. B **106**, L100502 (2022).
[59] P. Dutta and A. M. Black-Schaffer, Signature of odd-frequency equal-spin triplet pairing in the Josephson current on the surface of Weyl nodal loop semimetals, Phys. Rev. B **100**, 104511 (2019).
[60] R. Seoane Souto, D. Kuzmanovski, and A. V. Balatsky, Signatures of odd-frequency pairing in the Josephson junction current noise, Phys. Rev. Res. **2**, 043193 (2020).
[61] T. S. Khaire, M. A. Khasawneh, W. P. Pratt, and N. O. Birge, Observation of spin-triplet superconductivity in Co-based Josephson junctions, Phys. Rev. Lett. **104**, 137002 (2010).
[62] A. Di Bernardo, S. Diesch, Y. Gu, J. Linder, G. Divitini, C. Ducati, E. Scheer, M. G. Blamire, and J. W. Robinson, Signature of magnetic-dependent gapless odd frequency states at superconductor/ferromagnet interfaces, Nat. Commun. **6**, 8053 (2015).
[63] S. Hart, H. Ren, T. Wagner, P. Leubner, M. Mühlbauer, C. Brüne, H. Buhmann, L. W. Molenkamp, and A. Yacoby, Induced superconductivity in the quantum spin Hall edge, Nat. Phys. **10**, 638 (2014).
[64] C. Brüne, A. Roth, H. Buhmann, E. M. Hankiewicz, L. W. Molenkamp, J. Maciejko, X.-L. Qi, and S.-C. Zhang, Spin polarization of the quantum spin Hall edge states, Nat. Phys. **8**, 485 (2012).
[65] S. Das and S. Rao, Spin-polarized scanning-tunneling probe for helical Luttinger liquids, Phys. Rev. Lett. **106**, 236403 (2011).

[66] L. Fu and C. L. Kane, Josephson current and noise at a superconductor/quantum-spin-Hall-insulator/superconductor junction, Phys. Rev. B **79**, 161408(R) (2009).

[67] L. Fu and C. L. Kane, Superconducting proximity effect and Majorana fermions at the surface of a topological insulator, Phys. Rev. Lett. **100**, 096407 (2008).

[68] C. L. Kane and E. J. Mele, Quantum spin Hall effect in graphene, Phys. Rev. Lett. **95**, 226801 (2005).

[69] A. Calzona and B. Trauzettel, Moving Majorana bound states between distinct helical edges across a quantum point contact, Phys. Rev. Res. **1**, 033212 (2019).

[70] F. Keidel, S.-Y. Hwang, B. Trauzettel, B. Sothmann, and P. Burset, On-demand thermoelectric generation of equal-spin Cooper pairs, Phys. Rev. Res. **2**, 022019(R) (2020).

[71] A. Mukhopadhyay and S. Das, Thermal signature of the Majorana fermion in a Josephson junction, Phys. Rev. B **103**, 144502 (2021).

[72] A. Mukhopadhyay and S. Das, Thermal bias induced charge current in a Josephson junction: From ballistic to disordered, Phys. Rev. B **106**, 075421 (2022).

[73] D. Wadhawan, K. Roychowdhury, P. Mehta, and S. Das, Multi-electron geometric phase in intensity interferometry, Phys. Rev. B **98**, 155113 (2018).

[74] The azimuthal angle is of no consequence; e.g., it can also be assumed in the z-y plane.

[75] See Supplemental Material at http://link.aps.org/supplemental/10.1103/PhysRevB.109.L220504 for detailed derivations and additional information: Section A provides the derivation of the scattering matrices used in this Letter, Sec. B presents the derivation of Eq. (7) in terms of pairing amplitudes, Sec. C includes detailed expressions for different transmission amplitudes and free Green's functions, and, finally, Sec. D outlines the dependence of $\mathcal{A}$ on system parameters.

[76] S. S. Pershoguba, T. Veness, and L. I. Glazman, Landauer formula for a superconducting quantum point contact, Phys. Rev. Lett. **123**, 067001 (2019).

[77] C. W. Groth, M. Wimmer, A. R. Akhmerov, and X. Waintal, Kwant: A software package for quantum transport, New J. Phys. **16**, 063065 (2014).

[78] B. A. Bernevig, T. L. Hughes, and S.-C. Zhang, Quantum spin Hall effect and topological phase transition in HgTe quantum wells, Science **314**, 1757 (2006).

[79] J. Alicea, New directions in the pursuit of Majorana fermions in solid state systems, Rep. Prog. Phys. **75**, 076501 (2012).

[80] H. Li, L. Sheng, R. Shen, L. B. Shao, B. Wang, D. N. Sheng, and D. Y. Xing, Stabilization of the quantum spin Hall effect by designed removal of time-reversal symmetry of edge states, Phys. Rev. Lett. **110**, 266802 (2013).

[81] V. Adak, K. Roychowdhury, and S. Das, Spin-polarized voltage probes for helical edge state: A model study, Phys. E **139**, 115125 (2022).

[82] V. Adak, A. Mukhopadhyay, S. J. De, U. Khanna, S. Rao, and S. Das, Chiral detection of Majorana bound states at the edge of a quantum spin Hall insulator, Phys. Rev. B **106**, 045422 (2022).